DOI: 10.2195/lj_Proc_kivelae_en_201605_01
URN: urn:nbn:de:0009-14-43748

Simulation and analysis of an emergency lowering system for crane applications

Simulation und Analyse eines Notfall-Absenksystem für Krananwendungen

Tommi Kivelä
Markus Golder

Institut für Fördertechnik und Logistiksysteme (IFL)
Karlsruhe Institute of Technology (KIT)

An emergency lowering system for use in safety critical crane applications is discussed. The system is used to safely lower the payload of a crane in case of an electric blackout. The system is based on a backup power source, which is used to operate the crane while the regular supply is not available. The system enables both horizontal and vertical movements of the crane. Two different configurations for building the system are described, one with an uninterruptible power source (UPS) or a diesel generator connected in parallel to the crane's power supply and one with a customized energy storage connected to the intermediate DC-link in the crane. In order to be able to size the backup power source, the power required during emergency lowering needs to be understood. A simulation model is used to study and optimize the power used during emergency lowering. The simulation model and optimizations are verified in a test hoist. Simulation results are presented with non-optimized and optimized controls for two example applications: a paper roll crane and a steel mill ladle crane. The optimizations are found to significantly reduce the required power for the crane movements during emergency lowering.

[Keywords: emergency lowering, safety, crane, modeling, simulation]

1 Introduction

Cranes are an inseparable part of the process industry. The construction of new plants in industries like steel and paper production are increasingly focused to developing parts of the world. The electrical grid in these countries is often not as reliable as for example in Europe, and electrical blackouts can occur frequently. In some applications, such as handling hazardous materials, molten steel or paper rolls, leaving the payload hanging for the duration of a blackout can cause a significant safety risk. This paper describes a backup power source-based emergency lowering system, which can be used to safely operate the crane and lower the load during a power outage. The two example applications discussed in this paper are steel mill ladle cranes, used for handling molten steel, and automated storage cranes for unpacked paper rolls, which use vacuum pump-based lifting units for grabbing the paper rolls. For these two example applications, just lowering the load is not enough, it might also need to be moved horizontally for safe lowering.

1.1 Previous work

To the author's knowledge, no previous publications exist regarding emergency lowering systems for cranes. Currently some cranes are equipped by means of lowering the load in place. For example, the hoist can be equipped with a mechanism for forcing the hoist brake open during a power outage. In this case the payload can be lowered in place, but the operation might damage the brake. The system described in this paper is designed to also enable the traveling of the crane.

1.2 Objectives

In order to understand the electrical power required for the emergency lowering, a model of the crane electric motor drives is described and built. The characteristics of the power demand need to be understood in order to be able to define the requirements for the backup power source. The simulation models are used to test optimization methods to minimize the required power and thus the cost of the backup power source.

Two different configurations for connecting the backup power source to the crane electrics are described, one where the backup power source is in parallel to the regular supply grid and one where it is connected directly to the intermediate DC-link of the crane's electric drives. The benefits and disadvantages of both configurations are discussed.

The simulation model and the suggested optimizations are verified by measurements in a test hoist. The simulation model is used to simulate emergency lowering scenarios for the two example applications: for a paper roll crane with 15-ton nominal load and for a steel mill crane with a combined nominal lifting capacity of 470 tons. The simulations are presented with non-optimized and optimized control scenarios.

DOI: 10.2195/lj_Proc_kivelae_en_201605_01
URN: urn:nbn:de:0009-14-43748

2 ELECTRIC DRIVES IN CRANES

The example cranes discussed in this work are indoor overhead electric bridge cranes. The motor drives which power the movements of the cranes are electric, consisting of frequency converter-controlled induction motors. In this chapter the mechanical and electrical characteristics and the models used for the simulations in this work are described. The indirect vector control scheme for the induction motor is briefly introduced, as well as some motor control issues relevant to crane drives. The optimization methods used for the emergency lowering operation are discussed.

2.1 MECHANICAL CHARACTERISTICS

A gantry crane has two main types of electric drives, traveling drives for horizontal movement and hoist drives for vertical movement. The traveling drives are either bridge drives for moving the crane bridge along the runway or trolley drives for moving the trolley along the bridge. The load characteristic for the hoist drive is constant load torque with low friction and inertia. The traveling drives torque profile is characterized by moderate to high inertia and load torque from friction and load swing. The differing characteristics translate into differing power requirements.

The mechanical dynamics of a motor drive are shown in equation (1).

$$J\frac{\mathrm{d}\omega_\mathrm{m}}{\mathrm{dt}} = T_m - T_{load} \tag{1}$$

In the equation, J is the total inertia of the drive, ω_m is the mechanical angular speed of the motor, T_m is the torque produced by the motor, T_{load} is the torque caused by the load. When driving at constant speed, the motor torque will be equal to the load torque. When lifting the load up with the hoist drive, potential energy is being stored, which will be released when lowering the load. When accelerating or decelerating, kinetic energy is stored into or restored from the system.

From equation (1), the mechanical power of the system can be obtained as shown in equation (2).

$$\begin{aligned} P_m &= \omega_\mathrm{m} T_m = \omega_\mathrm{m} T_{load} + \omega_\mathrm{m} J\frac{\mathrm{d}\omega_\mathrm{m}}{\mathrm{dt}} \\ &= P_{constant} + P_{dynamic} \end{aligned} \tag{2}$$

For the emergency lowering applications, the optimization goal is to minimize the power required by the drives to complete the necessary movements in order to lower the payload down during a power cut. Therefore the maximum power required by each movement is studied. During regular operation, the maximum power required by the hoist drive is at the end of acceleration when lifting the load. Similarly for the traveling drives, the maximum power is consumed when accelerating the motion. When lowering the load, the hoist drive is operating in regenerating mode, and the power flows back to the drive instead of being consumed. In this work the efficiency of the drive mechanics is considered as a single parameter, the total mechanical efficiency, η. When the drive is operating in the motoring mode, such as when the hoist drive is lifting a load or when a traveling drive is accelerating or driving at constant speed, the total mechanical efficiency increases the mechanical power required from the drive, as shown in equation (3). When the drive is operating in the regenerating mode, such as when the hoist drive is lowering the load or when a traveling drive decelerates a motion, and the kinetic energy stored in the system flows back to the drive, the total mechanical efficiency reduces the mechanical power to the drive, as shown in equation (4).

$$T_{m-motoring} = \frac{1}{\eta}\left(T_{load} + J\frac{\mathrm{d}\omega_\mathrm{m}}{\mathrm{dt}}\right) \tag{3}$$

$$T_{m-regenerating} = \eta\left(T_{load} + J\frac{\mathrm{d}\omega_\mathrm{m}}{\mathrm{dt}}\right) \tag{4}$$

In the hoist drive the load torque is constant and caused by the load hanging in the hook. Compared to the load torque, the friction torque is small, and is not taken into account in the hoist drive simulations in this work. In the traveling drives the load torque caused by friction can be modeled as a constant torque, opposite in sign to the mechanical speed, with slight increase toward a discontinuity at zero speed [Mit12; Har08]. In this work the friction torque model for the traveling drives only consists of the static friction, the increase in the friction around zero speed is not taken into account. For the traveling drives, the relevant simulation results are the maximum power values during acceleration and the constant speed power, for which the simplified friction model does not have a significant effect.

2.2 ELECTRICAL MODEL

For modern process cranes, the electrical drives are typically frequency converter-controlled induction motors. For larger cranes, the drives use a common DC-link. All the inverter bridges supplying the induction motors are connected to the same DC-link, which is supplied by one or more active front-end converters. When a single motor drive is consuming power, or operating in motoring mode, the power is supplied from the DC-link. When the motor is operating in regenerating mode, the power flows back to the DC-link. To prevent the DC-link voltage from increasing to levels which might damage the frequency converters' electronics, the excess power must be supplied back to the grid. However, the excess power can also be consumed by the other drives connected to the same DC-link.

Space vector-based modeling and control is used in frequency converter drives, where good dynamic performance is required. In space vector modeling a three-phase

DOI: 10.2195/lj_Proc_kivelae_en_201605_01
URN: urn:nbn:de:0009-14-43748

system is converted into an equivalent system of two perpendicular phases, presented by a single complex value. Only the zero frequency, or average component of the three phases is lost in the transformation, which is not typically present in motors. The space vector of the stator voltage of a motor in the stationary reference frame, $\underline{u}_s^s$, can be calculated as shown in equation (5), where j is the imaginary unit and u_a, u_b and u_c are the three phase voltages. The instantaneous active power of the motor can be calculated from the voltage and current space vectors as shown in equation (6) [Vas92].

$$\underline{u}_s^s(t) = \frac{2}{3}\left(u_a(t) + e^{\frac{j2\pi}{3}}u_b(t) + e^{\frac{j4\pi}{3}}u_c(t)\right) \quad (5)$$

$$p_s(t) = \frac{3}{2}Re\{\underline{u}_s^s(t)\left(i_s^s(t)\right)^*\} = u_a(t)i_a(t) + u_b(t)i_{b(t)} + u_c(t)i_c(t) \quad (6)$$

For control purposes, the space vector quantities are often transformed into an arbitrary reference frame, which means that the space vector is projected onto an axis rotating at some arbitrary angular speed, ω_g. Typical choices for the reference frames are ones which rotate synchronously with the stator voltage vector's angular speed, ω_s, or with the rotor flux vector's angular speed, ω_R. Equation (7) shows the transformation of the stator current vector from the stationary reference frame, i_s^s, to the rotor flux reference frame, $\underline{i}_s$. In the rotor flux reference frame, the real and imaginary parts of the space vector are denoted as the d- and q-components, respectively.

$$\underline{i}_s = \underline{i}_s^s e^{-jArg\{\underline{\psi}_R^s\}} = \underline{i}_s^s e^{-j\int\omega_R} = \underline{i}_s^s e^{-j\theta_R} = i_d + ji_q \quad (7)$$

The induction motors were modeled using the inverse-Γ equivalent circuit, which is shown in Figure 1. In the model the leakage inductance in the motor is presented by a single leakage inductance on the stator side. The model parameters are listed in Table 1. The inverse-Γ model loses no information compared to the traditional T-model, but is less complex and more suitable for control design purposes [Sle89]. The equivalent circuit can be described using the stator current $\underline{i}_s^s$ and the rotor flux $\underline{\psi}_R^s$ as state variables, as shown in equations (8)-(9). The torque is produced in the motor through interaction of the rotor flux and the current in the stator windings and can be calculated as shown in equation (10) [Har03]. The electrical rotor frequency is equal to the mechanical rotor frequency multiplied by the number of pole pairs in the motor: $\omega_r = p\omega_m$. [Har03]

$$\frac{d\underline{i}_s^s}{dt} = \frac{1}{L_\sigma}\left(\underline{u}_s^s - (R_s + R_R)\underline{i}_s^s - \left(j\omega_r - \frac{R_R}{L_M}\right)\underline{\psi}_R^s\right) \quad (8)$$

$$\frac{d\underline{\psi}_R^s}{dt} = R_R\underline{i}_s^s + \left(j\omega_r - \frac{R_R}{L_M}\right)\underline{\psi}_R^s \quad (9)$$

$$T_m = \frac{3p}{2}Im\{\underline{\psi}_R^{s*}\underline{i}_s^s\} \quad (10)$$

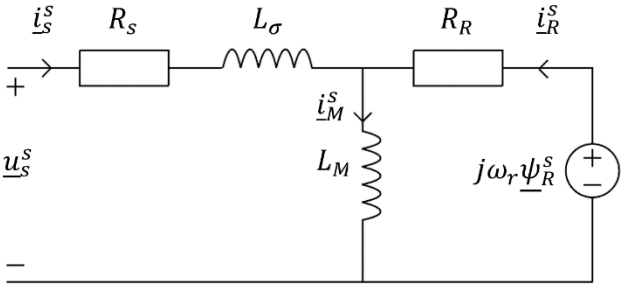

Figure 1. The Inverse-Γ equivalent circuit.

Table 1. Inverse-Γ equivalent circuit parameters.

Stator resistance	R_s
Total leakage inductance	L_σ
Rotor resistance	R_R
Magnetizing inductance	L_M

2.3 INDIRECT VECTOR CONTROL OF THE INDUCTION MOTOR

In vector control, the magnetization and torque production of the induction motor is controlled separately, as traditionally done with DC-motors. As will be shown next, the magnetization and the torque production can be controlled by the stator current components i_d and i_q in the rotor flux reference frame, respectively. To transform the stator current to the rotor flux reference frame, the rotor flux angle must be either estimated or measured. In direct vector control, the rotor flux is directly estimated or measured and then used to obtain the required transformation angle. In indirect vector control, as used in the simulation model in this work, the rotor flux is not directly estimated. Instead, the angular speed of the rotor flux is calculated using measured stator currents and rotor angular velocity and then integrated to obtain the rotor flux transformation angle. Converting the equation (9) to the rotor flux reference frame, and separating the result into real and imaginary parts yields the well-known relations shown in equations (11) and (12). The equations show that the rotor flux and the motor slip, and thus the torque production, can be controlled separately by controlling the current components i_d and i_q, respectively. Note that in rotor flux reference frame the rotor flux is real-valued. [Har03]

$$\frac{d\psi_R}{dt} = R_R i_d + -\frac{R_R}{L_M}\psi_R \quad (11)$$

DOI: 10.2195/lj_Proc_kivelae_en_201605_01
URN: urn:nbn:de:0009-14-43748

$$\omega_{sl} = \omega_s - \omega_r = \frac{R_R i_q}{\psi_R} \tag{12}$$

The magnetizing current reference is chosen as $i_d^{ref} = \frac{\psi_R^{ref}}{L_M}$. The torque produced by the motor, as expressed in equation (10), can be expressed in the rotor flux reference frame, as shown in equation (13). This relation can be used to calculate the reference of torque producing current i_q^{ref} as function of the torque and flux reference, as shown in equation (14).

$$T_m = \frac{3p}{2} Im\{\psi_R \underline{i}_s\} = \frac{3p}{2} \psi_R i_q \tag{13}$$

$$i_q^{ref} = \frac{2}{3p} \frac{T_m^{ref}}{\psi_R^{ref}} \tag{14}$$

The rotor flux transformation angle θ_R can be calculated by integration from equation (12) by substituting ψ_R and i_q with their respective reference values, as shown in equation (15) [Har03].

$$\theta_R = \int \omega_r + \omega_{sl} = \int \omega_r + \frac{R_R i_q^{ref}}{\psi_R^{ref}} \tag{15}$$

The full indirect vector control system is shown in Figure 2. The stator current and the rotor speed are used as feedback to the control system. The rotor flux reference frame transformation angle and the current reference components are calculated based on the speed feedback and the flux and torque references. The torque reference is the output from the speed controller. The speed controller used in the simulation model is a regular PI-controller. The flux reference is a constant value, since field weakening is not used in the simulations in this work. The current controller used in the simulations is a synchronous frame complex-valued PI-controller with inner decoupling and an active damping loop as described by [Har03] and shown in equations (16)-(18).

$$\underline{e_i} = \underline{i}_s^{ref} - \underline{i}_s \tag{16}$$

$$\frac{d\underline{I}}{dt} = \underline{e_i} \tag{17}$$

$$\underline{u}_s^{ref} = k_p \underline{e_i} + k_i \underline{I} + (j\omega_s L_\sigma - R_a)\underline{i}_s \tag{18}$$

The voltage reference is obtained as the output from the current controller. The voltage reference is transformed to the stationary reference frame. In actual applications the inverter would produce the voltage reference using pulse-width or space vector-based modulation scheme. In the simulation model the voltage reference is used directly as the input of the induction motor model.

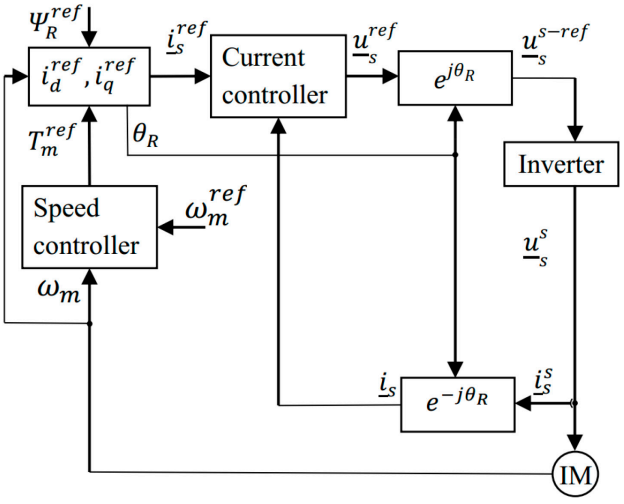

Figure 2. Indirect vector control

2.4 SPECIFICS OF MOTOR CONTROL IN CRANES

Crane drives are equipped with electromechanical holding brakes, which prevent the hoist load from dropping or the bridge or trolley from traveling while the drive is not active. The control of the electromechanical brakes is tightly coupled with the motor control. Especially in hoisting, the brake needs to be controlled properly to prevent load slipping in starts and stops. An example of the start and stop control is shown in Figure 3.

In order for the motor to be able to produce sufficient torque, the rotor flux is built up to the nominal value prior to brake opening. This start magnetization is usually done with a pre-defined current value. In order to build the nominal flux, the current must be at least equal to the nominal flux current, or no-load current, of the motor. However, usually a higher current value will be used, for example in the range of 100% to 120% of the motor nominal current, to build the flux faster and time-optimize the start operation. Equation (11) shows that in the rotor flux reference frame the rotor flux has first order dynamics with the rotor time constant $\tau_R = L_M/R_R$. Assuming constant magnetizing current reference i_d^{ref} the rise time to flux reference ψ_R^{ref} can be solved from equation (11) and calculated as shown in equation (19). The equation does not take current rise time into account, but can be used to estimate the flux build-up time with sufficient accuracy.

$$t_{magnetization} = -\tau_R \ln\left(\frac{L_M i_d^{ref} - \psi_R^{ref}}{L_M i_d^{ref}}\right) \tag{19}$$

The operation of the electromechanical brake has delays due to the operation of the brake itself and the relays and contactors in the control circuitry feeding the brake. The brake opening and closing delays must be taken into account in the motor control during the starts and stops. The goal of brake control is to open up the brake as soon as the

DOI: 10.2195/lj_Proc_kivelae_en_201605_01
URN: urn:nbn:de:0009-14-43748

motor magnetization is complete. Typically the magnetization time is slightly shorter than the brake opening delay. In this case the brake is controlled open immediately when the magnetization starts, and the motor is zero speed controlled, or floated, during the time difference while waiting for the brake to be fully open. If the magnetization time would be longer than the brake opening delay, the brake can be controlled to open simultaneously as the start magnetization is finished.

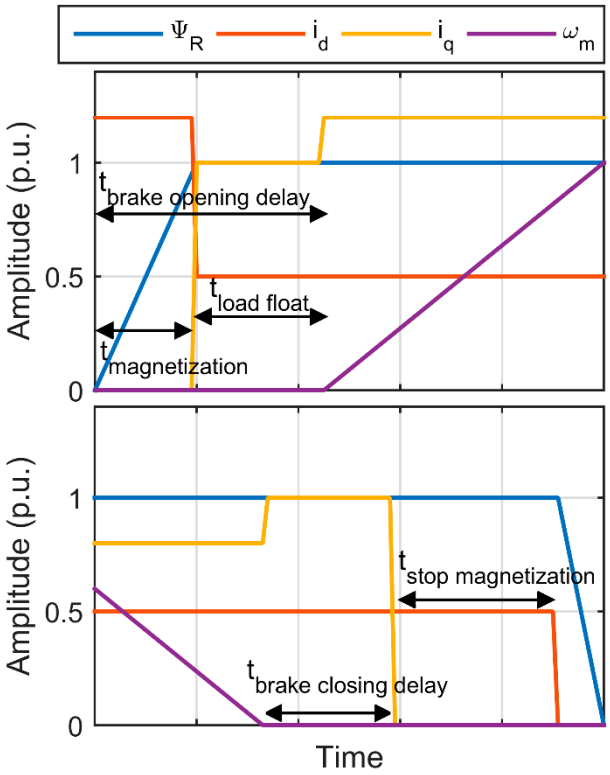

Figure 3. Example of the start and stop operation. The magnetizing current i_d is initially higher to increase the rotor flux ψ_R to the nominal value. Once magnetized, the torque producing current i_q is increased to produce torque to float the motor prior to brake opening. After brake opening, the mechanical speed ω_m is controlled to the reference. During stop the operation is reversed.

When the motion is run to a stop, the operation is similar, but reverse to the start sequence. The motor is controlled at zero speed for the duration of the brake closing delay. After the brake is closed, stop magnetization is used. In stop magnetization the motor is kept magnetized by supplying the motor with the nominal flux current. Stop magnetization is used in order to be able to start the movement quickly again if the user requests to do so, as the motor is already magnetized and only the brake needs to be opened. For a similar reason, sometimes the zero speed control period prior to brake closing is extended for a similar reason. This operation is called load floating.

2.5 Optimizing power usage for emergency lowering

To minimize the required size and cost of the emergency backup power source, methods for minimizing the power required by the drives during emergency lowering are studied. The main two methods used are:

- Optimization of the start and stop sequences, especially for the hoist drive and load lowering, by adjusting the start magnetization and by minimizing load floating by adjusting the brake control.
- Minimizing the mechanical power required in the traveling movements.

As discussed previously, for safety reasons it is required that the motor is magnetized to nominal motor flux prior to brake opening for the motor to be able to produce nominal torque. For lowering, even smaller than nominal flux would be sufficient for brake starting, since the torque required in the regenerating mode is smaller than in motoring mode, meaning that further optimization could be done. In this work, however, the nominal flux is required to ensure safety. During the start magnetization the motor consumes active power not only due to copper losses but as well from energy being stored to the magnetic field of the motor. The faster the flux is being built, the higher the momentary power required. The power for the copper losses also increase quadratically in relation to the current. Reducing the current from 100% - 120% of nominal current to a value equal to the nominal flux current slows down the flux build-up and the motion start, but yields significant power reduction for the hoist drive, as will be shown with measurements and simulations.

The motor drive starts consuming active power towards the end of the deceleration, when the regenerated power decreases to a value smaller than the drive losses. The drive is operating in the motoring mode during the load floating operation and active power is consumed by the copper losses during the stop magnetization. The power required by the stop magnetization is equal to the power required by the optimized version of the start magnetization, so further optimization is not required. However, for the optimized version, the load floating during stop will not be used to prevent power consumption. In addition, the hoist brakes will be controlled to close slightly before the zero speed has been reached, at a point where the drive is making the transition from regenerating to motoring mode. In regular operation this type of control would cause the hoist brakes to wear out unnecessarily fast, but for the emergency operation this is acceptable.

The most effective way to reduce the power required by the traveling drives is to minimize the mechanical power of the movements. In equation (2), the maximum mechanical power is required at the end of an acceleration ramp

DOI: 10.2195/lj_Proc_kivelae_en_201605_01
URN: urn:nbn:de:0009-14-43748

and is directly related to the final speed and to the inverse of the acceleration time. Reducing the allowed maximum speed and increasing the acceleration times are sufficient methods to significantly reduce the power required by the traveling drives for emergency lowering.

3 EMERGENCY LOWERING SYSTEM

The purpose of the emergency lowering system is to provide sufficient power to operate the crane safely in the case of an electric blackout to lower the crane's payload down into a safe place to prevent the danger or damage which might be caused if the payload is not lowered. The system safety is briefly discussed and two different configurations to build the system are suggested.

3.1 SAFETY

The safety requirements for cranes sold in Europe are set by the European machinery directive [EU06]. For cranes sold outside of Europe, several international standards give guidance for the safety requirements. The included emergency lowering system must fulfill the same set of requirements as the whole crane. The backup power source needs to be designed such, that it will supply all the auxiliary circuitry of the crane in addition to the electric drives. This increases the required constant power from the backup power source, but all the safety-related circuitry of the crane will be active and therefore guarantee safe operation.

The standard EN ISO-12100, which defines basic safety concepts and general principles, includes the description for unexpected start-up, which is "any start-up which, because of its unexpected nature, generates a hazard", which can be caused, for example by the "restoration of the power supply after an interruption" [ISO12100]. If an automatically operating crane would start moving after a power cut, powered from the backup power source, without explicitly being activated, it can be considered an unexpected start-up. Therefore, the emergency lowering system must be designed in such a way, that there is a method for separately activating the system to prevent an unexpected start-up.

3.2 SYSTEM CONFIGURATIONS

Two different configuration types are shown in Figure 4 and Figure 5. In the first configuration the backup power source is connected in parallel to the power grid. This type of system configuration can be built using either an offline-type uninterruptible power source (UPS) or a diesel generator. UPS-devices are also available in an on-line configuration, where the device is in series between the power grid and the supplied load [Gur07]. The advantage of the offline-type UPS for this applications is that the backup power source can be sized according to the power need in the emergency situation, as opposed to the online-type UPS, which would need to be sized according to the full power of the crane in regular operation. The emergency lowering system would not be economically feasible with an online-type UPS. The benefit of this configuration is, that it can be built using standard, non-customized, components. In addition to the backup power source a braking chopper and a resistor bank need to be included into the DC-link to handle excess energy when the drives operate in the regenerating mode. This is necessary, since UPS-devices do not support regenerative mode loads as the lead acid-batteries still used today do not support quick charging [Ito10]. Naturally, diesel generators are also not able to absorb a significant amount of power from the load.

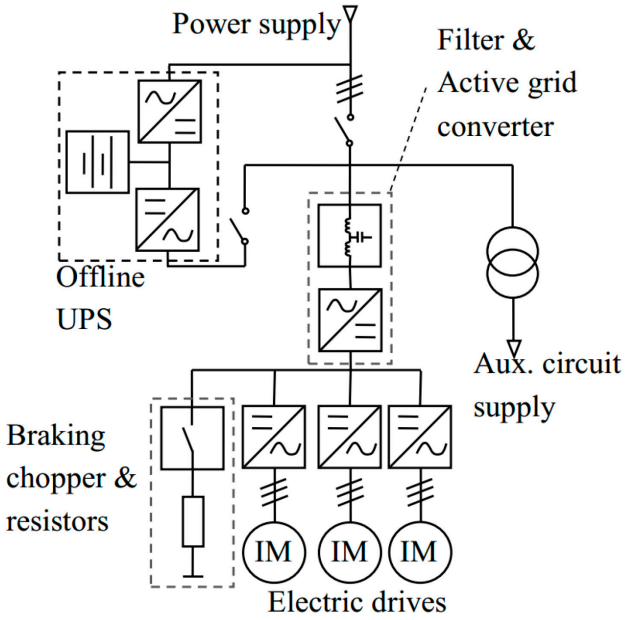

Figure 4. First system configuration: A back-up power source in parallel to the grid.

The sizing of a UPS-device or a diesel generator requires knowing the constant and the maximum power of the supplied load. Typical overload-capability for a UPS-device is 150% for 5-10 seconds or 200% for less than a second [Eaton12]. For a diesel generator designed for standby-operation, overloading is not typically not supported [Ive07]. Thus, UPS-devices could provide more flexibility in the sizing.

In the second configuration, as shown in Figure 5, the backup power source is an energy storage directly connected to the DC-link via a separate DC-DC-converter. In this configuration the backup power source could utilize either or both super-capacitors and batteries for handling momentary high power. This configuration requires additional converter for creating the supply voltage for the auxiliary circuits. Energy from drives operating in regenerative modes can be partly used to recharge the energy storage, but a braking chopper and resistor bank are also needed for cases where the regenerated power is higher than can be

DOI: 10.2195/lj_Proc_kivelae_en_201605_01
URN: urn:nbn:de:0009-14-43748

used for loading the energy storage or when the energy storage is already at full capacity. The system is more complex and is more likely to require customized components than the first configuration, but offers more flexibility in sizing and optimization.

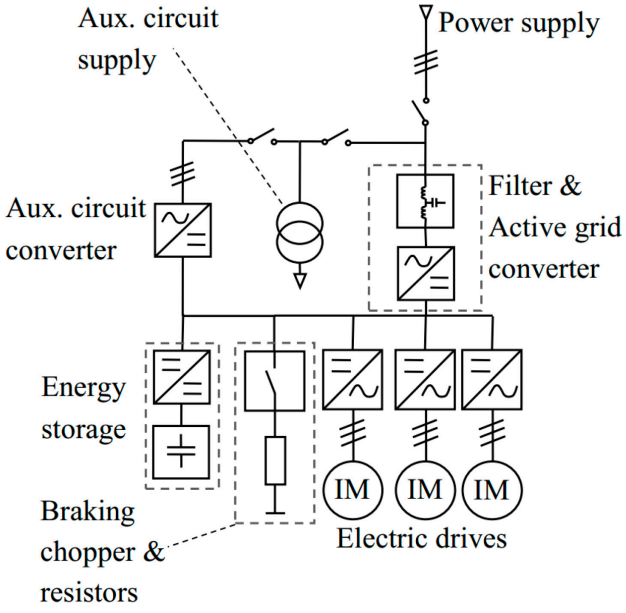

Figure 5. Second system configuration: Energy storage connected to the DC-link.

3.3 SIZING OF THE BACKUP POWER SOURCE

In order to determine the required power for the backup source, the following parameters need to be defined:

- Required constant power: The power required by the control circuitry and possible auxiliary circuitry, such as crane lights, and the constant losses in the electric drives.
- Required dynamic power: The power required by the drives, initial charging of the DC-link and then executing the crane movements define the dynamic power requirement.
- Required standby-time: How long the systems need to be powered during the emergency. The total energy capacity in the backup power source needs to be enough to provide the constant power for all of the standby time and also the energy required by the movements.

The nominal power and energy capacity of the backup power source will be defined based on the overload-capability of the selected source and by the power characteristic of the application.

4 SIMULATIONS

A model was built in Matlab Simulink for the simulation of electric drives in crane applications. The model consists of the model for an induction motor, an indirect vector control system and a simple mechanical model, with the dynamics as described in equation (1), together with simple models for the total mechanical efficiency, equations (3)-(4), and the drive brake. For all the simulations the total mechanical efficiency of the drives was assumed to be 85%. The brake model used in the simulations is simple, when the brake is applied it negates the effect of the motor and load torque to the axis and has a negative speed feedback loop with high gain to very quickly slow the speed to zero. The torque produced by the brake model is limited to 500% of the motor's nominal torque. The used model does not model an electromechanical brake properly, but is sufficient for the simulation purposes in this work.

The simulation model is verified by doing measurements and simulations for a test hoist. Two example applications discussed and simulated: a paper roll crane in an automated storage and retrieval system (AS/RS) for unpacked paper rolls and a steel mill ladle handling crane for transporting molten metal. For both examples the requirements for an emergency lowering system are described and simulations are presented and discussed with non-optimized and optimized controls.

4.1 MODEL VERIFICATION

The simulation model was verified by measurements in a test hoist drive, the details of which are shown in Table 2. The hoist was loaded with nominal load, which produced a load torque roughly equal to the motor nominal torque when the drive is operating in motoring mode. A digital oscilloscope was used to measure two phase-to-phase voltages and two phase currents. The voltage and current space vectors and further the active power were calculated from the results.

Measurements were taken from the beginning and ending of lowering motion with nominal load. Slowing to stop and stop magnetization takes a longer time than the beginning of the movement, so the sampling rate of the oscilloscope was reduced to be able to capture the whole sequence. This is visible as increased noise in the measurements of stop sequences compared to start sequences in Figure 6 and Figure 7.

Figure 6 shows the measurements and simulation results in the non-optimized case. When the lowering motion is started, a high current is used to quickly magnetize the motor prior to brake opening. The motor is floated until brake opening. After brake opening the lowering motion is accelerated. The figure shows that the simulation results are sufficiently close to the measurement. The measured voltage during the start magnetization and floating is slightly

DOI: 10.2195/lj_Proc_kivelae_en_201605_01
URN: urn:nbn:de:0009-14-43748

higher than the simulated result. The difference can be explained by long motor cables, since it is most visible in the low frequencies, where the cable resistance has a relatively higher effect compared to the inductance of the motor windings. The effect of the voltage difference is visible as slightly higher active power of the measurement during start magnetization. After the start magnetization, there is only a small error in the simulated active power compared to the measured one.

For stopping the lowering motion, the same difference in voltage level due to the long cabling at low driving frequency is visible. Also the measured current when floating the load and during stop magnetization is higher than the simulated one. This can be due to differences in the controllers of the actual drive compared to the simulation. The actual drive might have a small drift error in the rotor flux angle estimate, which results slightly higher current usage. However the error between the simulated and measured active power is again very small.

Similar simulations and measurements are shown in Figure 7 for the optimized case. The start sequence has been made longer by using only nominal magnetizing current of the motor for start magnetization. For the stop sequence, the brake is closed at such a driving frequency, that no load floating at zero speed takes place, only stop magnetization which requires very little power. As in the optimized case, the simulated and measured voltages and currents differ slightly, but the error in simulated active power is small.

Table 2. Test hoist motor data.

Motor nameplate values	
Nominal voltage	400 V
Nominal current	34 A
Nominal flux current	14.9 A
Nominal frequency	100 Hz
Nominal speed	2910 rpm
Nominal power	18 kW
Power factor, $\cos\varphi$	0.86
Nominal torque	59.1 Nm
Motor model parameters	
Stator resistance, R_s	128 $m\Omega$
Rotor resistance, R_R	149.5 $m\Omega$
Total leakage inductance, L_σ	1.9 mH
Magnetizing inductance, L_M	24.4 mH
Drive total inertia, J	0.0317 kgm^2

Comparing the active power of the non-optimized and optimized case shows that the required maximum power for load lowering can be reduced significantly from approximately 10% of motor nominal power to less than 2% for the test motor. The result is significant when considering backup power sources for hoist drives in the larger than 100kW range.

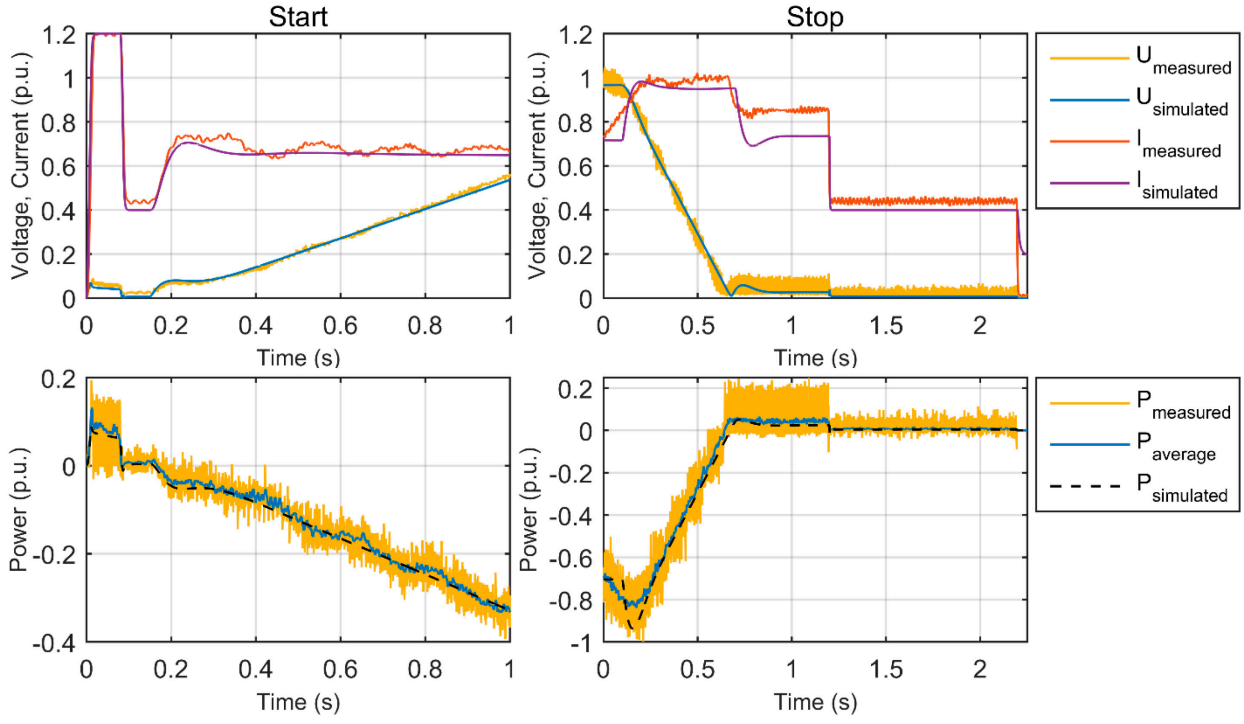

Figure 6. Hoist measurements against simulated results with non-optimized controls.

DOI: 10.2195/lj_Proc_kivelae_en_201605_01
URN: urn:nbn:de:0009-14-43748

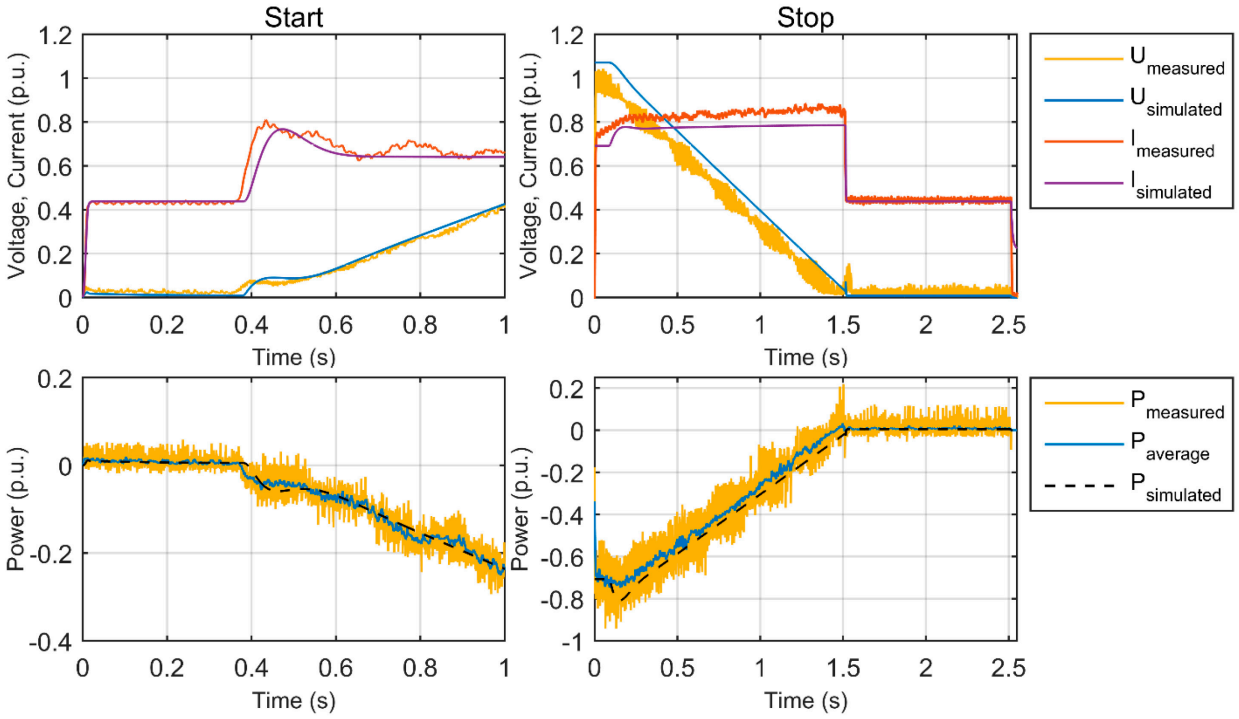

Figure 7. Hoist measurements against simulated results with optimized controls.

4.2 PAPER ROLL CRANE

The automated paper roll storage crane discussed here is for unpacked paper rolls. The crane operates automatically in a storage area containing stacks of unpacked paper rolls. The paper rolls are grabbed using a vacuum lifter unit (VLU) as a loading device, which grabs the paper rolls by utilizing vacuum pumps [Kon12]. Typically the cranes with this type of loading devices are already accompanied with a backup power sources for keeping the vacuum pumps running during power cuts [Kon15]. However, in case of a prolonged power cut, there is a risk of the paper roll falling.

The simulated crane has a nominal load of 15 tons. The hoisting machinery has one motor and an inverter. The bridge travel machinery consists of two motors and two inverters, one per each runway. The trolley travel machinery consists of two motors operated by a single frequency converter. The trolley motors are operated in scalar, or U/f control, but for this simulation the same closed loop model was used for the simulation since the active power of the drive will not differ significantly between the two control modes for the purposes of this work. All the electric drives are connected in a single DC-link. Information regarding the simulated paper roll crane drives is shown in Table 3.

In an emergency lowering situation the paper roll needs to be positioned on top of the closest possible stack and then lowered. Thus, the traveling movements cannot utilize the energy gained by lowering the load. The rolls are typically a maximum of two meters in diameter. When a roll is being moved in the storage space, it is initially lifted to the upper limit to ensure it will not collide with the other rolls. A typical total lifting height is 15 meters. To simulate the worst case need for positioning to on top of the closest roll stack in an emergency lowering situation, the traveling distance for both the trolley and the bridge was 2.5 meters. The simulated lowering distance was 15 meters. In the simulations, the crane is assumed to be carrying the nominal load.

Table 3. Simulated paper roll crane data.

Nominal load weight	11.4 $tons$
Loading device weight	3.6 $tons$
Nominal lifting speed	60 m/min
Nominal ramp time of the hoist	3 s
Number of hoisting motors	1
Nominal bridge traveling speed	120 m/min
Nominal ramp time of bridge traveling	5.5 s
Number of bridge traveling motors	2
Nominal trolley traveling speed	60 m/min
Nominal ramp time of trolley traveling	3s
Number of trolley traveling motors	2

The simulation results are shown in Figure 8. All the power values are scaled to the nominal power of the hoist motor. Since the traveling distance is relatively small, the position controller will not accelerate the traveling speed to

DOI: 10.2195/lj_Proc_kivelae_en_201605_01
URN: urn:nbn:de:0009-14-43748

the maximum speed even with non-optimized controls. The final speed reference with non-optimized controls for the bridge and the trolley was 33% of nominal.

The main goal of the optimization was to reduce the maximum required active power for the traveling movements. The maximum allowed speed for the traveling movements was further reduced to 20% of nominal speed for the bridge and 25% of the nominal speed for the trolley. The ramp times for both the bridge and the trolley were increased to 400% of nominal ramp time. For all drives the start magnetization is performed using nominal flux current instead of 120% of nominal current. For the hoist the mechanical brake is closed at 1.4Hz mechanical speed to prevent the drive from entering motoring mode, and thus from consuming power, at the end of the deceleration ramp.

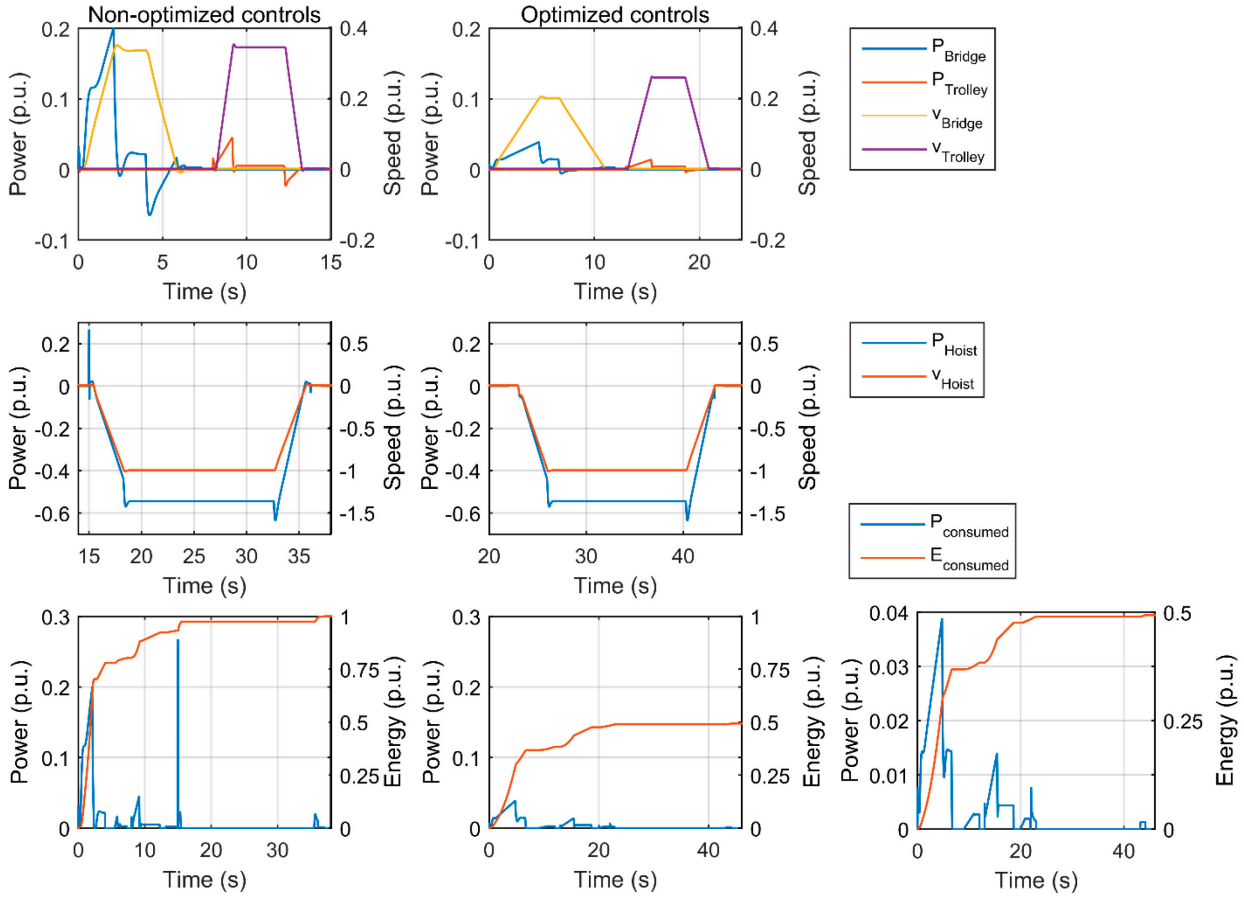

Figure 8. Paper roll crane simulation results. The optimized total power and energy is shown with a scaling similar to the non-optimized results for ease of comparison and with a scaling better adjusted to the waveforms.

With the optimization, the maximum active power consumed by the crane movements was reduced from 27% to less than 4% of the hoist motor nominal power. The total energy consumed by the drives was also reduced to approximately 50% of the value with non-optimized controls. Therefore, the simulation results show that the power requirement of the backup power source can be reduced significantly with the used optimizations.

The simulations show that a relatively small maximum power is required for the emergency lowering operation with the optimizations. The more suitable configuration choice for this type of crane would be the one shown in Figure 4, where the same UPS-device or diesel generator would provide backup power to the vacuum pumps and for the whole crane for the duration of the emergency lowering.

4.3 Steel Mill Crane

The example steel mill crane is a ladle handling crane used for moving molten metal from a process phase to the next [Kon14]. The total hoisting capacity is 360 + 110 tons. The ladle is handled by a main hoist (360 ton capacity) and an auxiliary hoist (110 tons) in separate trolleys. The main hoist is responsible for lifting the ladle and the auxiliary hoist is used for inclining the ladle in order to pour the metal out. The main and auxiliary hoist need to be hoisted

DOI: 10.2195/lj_Proc_kivelae_en_201605_01
URN: urn:nbn:de:0009-14-43748

and lowered synchronously to prevent inclining the ladle. Similarly, the main and auxiliary trolley must travel synchronously. All the drives in the crane utilize closed loop vector control and are connected to the same DC-link. Information regarding the simulated crane is shown in Table 4.

In case of a prolonged power cut, it is possible that molten metal left in the ladle can melt through and cause a hazardous situation and significant damage. Ideally the molten metal should be transported where it is safe to be poured out, for example to the next process phase. In an emergency lowering situation it will be possible to start the lowering and the traveling movements at the same time. Therefore the energy gained from lowering the load can be used for the traveling movements. The simulation was used to study how far the crane could travel in an emergency lowering situation and with how little power from the backup power source. It is again assumed that the crane is carrying the nominal payload.

The simulation results are shown in Figure 9. All the powers shown are scaled to the nominal power of the main hoist motors. For both the non-optimized and the optimized case, the traveling movements were started after the main and auxiliary hoists have reached the final speed and are regenerating power. In both simulations the crane nominal load is lowered 3 meters, the bridge travels 25 meters and the trolleys 15 meters. In the non-optimized case, the active power during bridge acceleration is higher than the power regenerated by the hoist movements. In addition, the trolley movements at nominal speeds take longer than the lowering operation and thus consume power when the load lowering stops. Therefore, the goal of the optimization is to fit the traveling movements into the time frame of the lowering operation in such a manner that all the power required by the traveling movements is provided by the regenerated power from the hoist drives.

For the optimization, the load lowering speed was reduced to 50% of nominal speed to extend the period of time when excess energy is available for traveling. In addition, the start magnetization of the hoist motors was performed using nominal flux current instead of 120% of nominal current as usually. The hoist brake is closed when the rotor speed is 1 Hz to prevent power consumption during the end of deceleration. For the traveling drives the start magnetization was not optimized for reduced power, since in this case the power comes from the lowering movement and it is beneficial to start the traveling as fast as possible. The maximum speed of the bridge was reduced to 50% of nominal, while the acceleration ramp was increased to 200% of nominal. For the trolleys, the maximum speed was reduced to 66% of nominal and the acceleration ramp was increased to 150% of nominal. The traveling and lowering distances were the same as for the non-optimized simulation. With the adjustments to the traveling movements, the total power of the crane movements stays negative during the whole load lowering. Therefore, the total power and energy consumed by the crane movements during the emergency lowering are during the start and stop of the hoist motors. With the optimized start magnetization the maximized power is less than 2% of the main hoist motor's nominal power. The result shows that by limiting the power of the traveling movements to use just what is available in the DC-link, the ladle can be moved significant distances just by utilizing the potential energy gained from the lowering movement.

Table 4. Simulated steel mill ladle crane data

Main hoist nominal payload	190 $tons$
Loading device weight	170 $tons$
Aux. hoist nominal payload	110 $tons$
Nominal lifting speed	6.3 m/min
Nominal ramp time of the main hoist	3.5 s
Number of motors in main hoist	2
Number of motors in aux. hoist	1
Nominal bridge traveling speed	80m/min
Nominal ramp time of bridge traveling	5 s
Number of bridge traveling motors	8
Nominal trolley traveling speed	30m/min
Nominal ramp time of trolley traveling	3.5 s
Number of main trolley traveling motors	4
Number of aux. trolley traveling motors	2

The steel mill crane needs only short momentary power bursts for the crane movements during the emergency lowering. Therefore for this the crane the better candidate would be the system configuration shown in Figure 5. The energy storage can provide the short power burst to start the emergency lowering and then be instantly recharged from the regenerated energy. Provided that the maximum power for the traveling movements are restricted properly, all the energy consumed by the crane can be supplied by the energy regenerated from the load lowering. However, with the system as described, the load cannot be hoisted up, and once the potential energy is consumed by lowering the load, further movements cannot be made. Therefore a major disadvantage of the system described here is that it does not allow major errors for the operator when handling the crane during emergency lowering.

DOI: 10.2195/lj_Proc_kivelae_en_201605_01
URN: urn:nbn:de:0009-14-43748

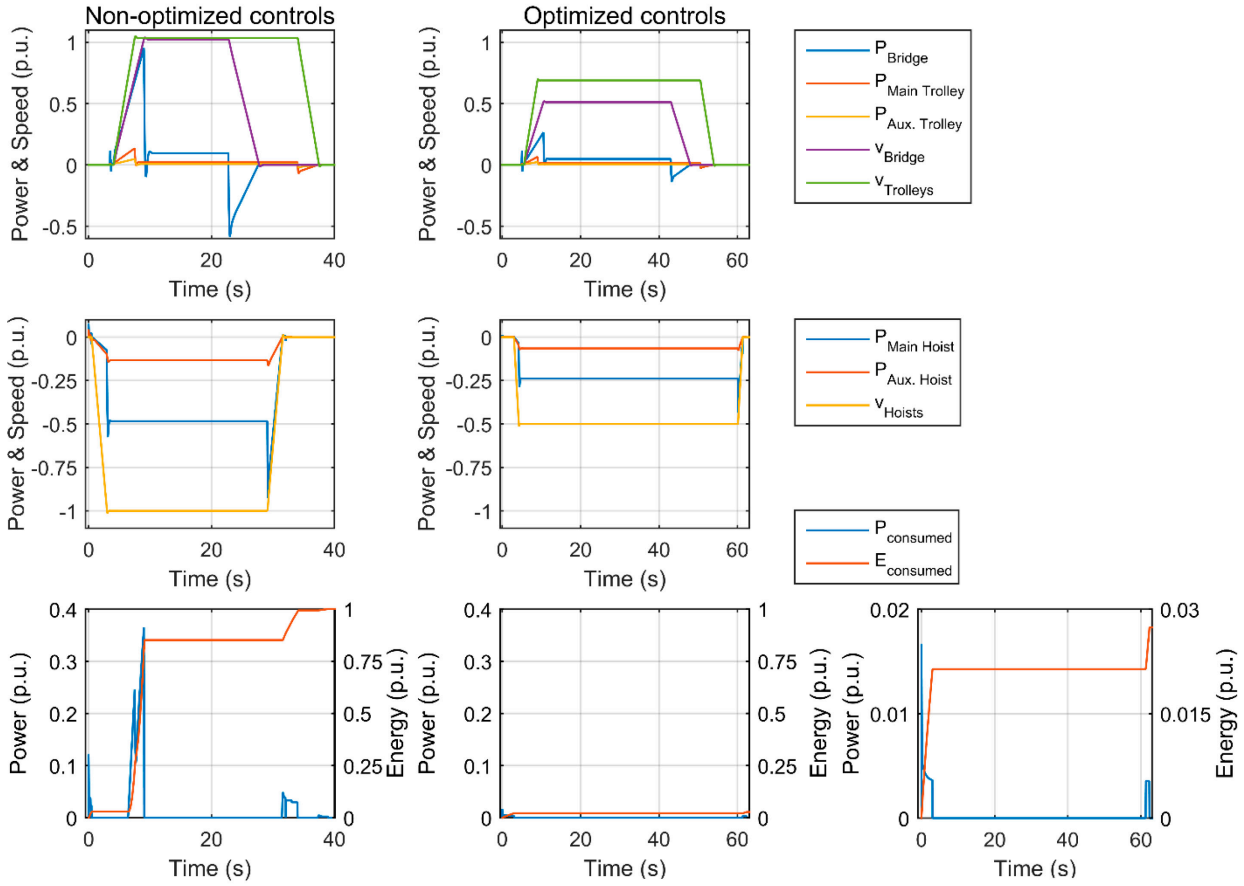

Figure 9. Steel mill crane simulation results. The optimized total power and energy is shown with a scaling similar to the non-optimized results for ease of comparison and with a scaling better adjusted to the waveforms.

5 Conclusions

In this paper, a concept for an emergency lowering system for crane applications was discussed. The system would enable the safe lowering of a crane's payload during an electric blackout. Such a system would be beneficial for applications, where leaving the payload hanging during a power cut can cause a significant hazard.

Two different configurations for the emergency lowering system were described. The first one configuration was based on UPS-devices or diesel generators, which would be connected in parallel to the cranes regular supply. The main advantage of this system is that commercial products can be utilized for the backup power source. The disadvantage of this setup is low support for customization. The second configuration was based on a customized energy storage, which would be connected directly to the DC-link of the crane drives. The benefit of the configuration is high customizability but with the disadvantage of higher costs of the customized components. For both configurations a braking unit and braking resistors need to be used for consuming excess energy, which increases the cost of the system.

The power consumption of the crane drives and optimization methods to reduce it were discussed. For the hoist drive the start and stop sequences were optimized by modifying the brake control and reducing the current used for initial motor magnetization. These methods were tested and verified by simulations. The simulation model and the optimizations were verified by measurements in a test hoist. The maximum power consumed by the test hoist during the start and stop sequence of a lowering movement was verifiably reduced from 10% to less than 2% of the motor's nominal power. For the traveling drives of the crane the mechanical power required by the movements was reduced by lowering the allowed speed and increasing the acceleration time.

The emergency lowering was simulated for two example applications, a paper roll crane and a steel mill crane. For the paper roll crane the traveling movements had to be done prior to load lowering. The maximum power required for the movements required for emergency lowering was reduced significantly with the optimizations, from 27% to 4% when scaled to the nominal power of the hoist motor. The energy consumed in the drive movements was reduced by 50%.

DOI: 10.2195/lj_Proc_kivelae_en_201605_01
URN: urn:nbn:de:0009-14-43748

For the steel mill crane the simulations showed that if the traveling movements are only performed by using the power available from the payload lowering, the payload can be moved significant distances with a relatively small backup power source, which only needs to be able to provide a power equal to 2% of the cranes hoist motor's nominal power. However, this method does not allow for significant operator errors, as once the load is lowered the system cannot supply power for further movements.

For future research, the simple models of the mechanical dynamics used in this work could be replaced by more accurate ones. Especially the traveling drive simulation results were not verified by measurements on actual equipment, where the friction and load swing can cause the load torque of the drive to behave differently from the constant load torque used in this work. More accurate electrical models could also be produced, as the efficiency of the power electronics in the drives was not taken into account, nor the losses in the motors, apart from the copper losses.

LITERATURE

[Eaton12] Eaton Corporation: *Whitepaper - Understanding UPS overload capabilities*. 2012. URL http://pqlit.eaton.com/ll_download_bylitcode.asp?doc_id=17866. Referred on 17.08.2015.

[EU06] European commission: *Directive 2006/42/EC on machinery*. URL http://eur-lex.europa.eu/LexUriServ/LexUriServ.do?uri=OJ:L:2006:157:0024:0086:EN:PDF. Referred on 17.08.2015.

[Gur07] Gurrero, J.M.; de Vicuna, L.G.; Uceda, J.: *Uninterruptible power supply systems provide protection.* Industrial Electronics Magazine, IEEE, vol.1, no.1, pp.28,38, Spring 2007.

[Har03] Harnefors, L.: *Control of Variable-Speed Drives*. Department of Electronics, Mälardalen University, Sweden, 2003.

[Har08] Harnoy, A.; Friedland, B.; Cohn, S.: *Modeling and measuring friction effects.* Control Systems, IEEE, vol.28, no.6, pp.82,91, Dec. 2008

[ISO12100] The European Committee for Standardization: *EN-ISO 12100: Safety of machinery – Basic concepts, general principles for design*.

[Kon12] Konecranes: *AS/RS solution for paper warehouses brochure*. URL http://www.konecranes.com/sites/default/files/download/automaticstorageandretrievalsystemsforpaperwarehouses.pdf. Referred on 11.08.2015.

[Kon14] Konecranes: *Steel eBook, Double girder ladle handling crane, p.60-61*. URL http://campaign.konecranes.com/steelbook/desktop/index.html. Referred on 11.08.2015.

[Kon15] Konecranes: *Paper roll vacuum lifters product sheet.* URL http://www.konecranes.com/sites/default/files/download/kc_vlu_product_leaflet_v9.pdf. Referred on 14.08.2015.

[Ito10] Ito, Y.; Ishiguma, S.: *Uninterruptible power supply with function of absorbing regenerative energy.* Power Electronics Conference (IPEC), 2010 International , vol., no., pp.1169,1173, 21-24 June 2010.

[Ive07] Cummins Power Generation, Iverson, J.: *Whitepaper – How to size a genset*. 2007. URL https://www.cumminspower.com/www/literature/technicalpapers/PT-7007-SizingGensets-en.pdf. Referred on 17.08.2015.

[Mit12] Mitrovic, N.; Petronijevic, M.; Kostic, V.;Jeftenic, B.: Electrical Drives for Crane Application, Mechanical Engineering, Dr. Gokcek, M. (Ed.), 2012. InTech. ISBN: 978-953-51-0505-3, DOI 10.5772/35560. URL http://www.intechopen.com/books/mechanical-engineering/electrical-drives-for-crane-application. Referred on 14.8.2015.

[Sle89] Slemon, G.R.: *Modelling of induction machines for electric drives*. Industry Applications, IEEE Transactions on vol.25, no.6, pp.1126,1131, Nov/Dec 1989.

DOI: 10.2195/lj_Proc_kivelae_en_201605_01
URN: urn:nbn:de:0009-14-43748

[Vas92] Vas, Peter: *Electrical machines and drives – A space-vector theory approach*. 1992, Oxford University Press - ISBN 0-19-859378-3.

M.Sc. Tommi Kivelä, is working as a Research associate at the chair of Safe mechatronic systems for intralogistics (SIMESI), Institute for material handling and logistics (IFL), Karlsruhe Institute of Technology (KIT).
E-mail: *Tommi.Kivelae@kit.edu*

Prof. Dr. -Ing. Markus Golder, is the head of the chair of Safe mechatronic systems for intralogistics (SIMESI), Institute for material handling and logistics (IFL), Karlsruhe Institute of Technology (KIT)
E-mail: *Markus.Golder@kit.edu*

Address: Institut für Fördertechnik und Logistiksysteme (IFL), Building 50.38, Gotthard-Franz-Str.8, 76131 Karlsruhe, Germany.
Tel.: +49 721-608-48621,
Fax: +49 721-608-48629.